Nonresonant Metasurface for Fast Decoding in Acoustic Communications

Xue Jiang,[1,2,3] Chengzhi Shi,[1] Yuan Wang,[1] Joseph Smalley,[1] Jianchun Cheng,[3] and Xiang Zhang[1,*]

[1] *Nano-scale Science and Engineering Center, University of California, Berkeley, California 94720, USA*
[2] *Department of Electronic Engineering, Fudan University, Shanghai, 200433, China*
[3] *Collaborative Innovation Center of Advanced Microstructures and Key Laboratory of Modern Acoustics, Institute of Acoustics, Department of Physics, Nanjing University, Nanjing 210093, China*

(Received 22 August 2019; published 9 January 2020)

Acoustic communication is crucial in underwater exploration, where sound is the dominant information carrier, with significantly less loss and scattering than that of electromagnetic waves. However, the capacity of acoustic communication channels is limited due to the intrinsically low speed of sound relative to that of electromagnetic waves and because the attenuation of acoustic waves underwater increases with frequency. Recently, orbital angular momentum (OAM) has emerged as an alternative multiplexing degree of freedom to encode data onto vortex beams for increasing the capacity of acoustic communication. For information retrieval from the multiplexed acoustic vortices, an active scanning method and a passive resonant method are explored. Time-consuming scanning and complex postprocessing significantly restrict the data-transmission speed, while the large amount of resonant cascaded devices in the passive technique intrinsically results in a low efficiency and bulky volume of the system. Here, we propose and experimentally demonstrate a passive and nonresonant approach with the ability to separate different OAM states of multiplexed acoustic vortex beams in parallel using a parabolic-phased metasurface. The metasurface converts the spiral-phase patterns of vortex beams carrying various angular momenta into plane waves with different in-plane linear momenta. Our approach is compatible with multiplexing technologies, significantly enhancing the speed in acoustic communication.

DOI: 10.1103/PhysRevApplied.13.014014

I. INTRODUCTION

Underwater communication plays an essential role in various applications, such as ocean environmental monitoring and offshore industrial exploration [1], where the rapidly increasing demands for high-definition signal transmission necessitate the high-speed transmission of megadata. Although remarkable progress has been achieved in wireless communications based on microwave or optical waves in air, electromagnetic communication technologies cannot be effectively adopted over a long distance underwater [2–4]. The prominent loss of microwaves intrinsically restricts radiofrequency communication to only several centimeters underwater, and the strong scattering of visible light caused by small particles inhibits optical waves from propagating over a long distance. Currently, acoustic waves are used as the dominant information carrier for underwater communication because the attenuation of acoustic waves is at least three orders of magnitude smaller (e.g., 7×10^{-4} dB/m at 0.15 m [5]) than that of electromagnetic waves (e.g., 2×10^{5} dB/m at 100 μm and 1 dB/m at 600 nm [6]). However, information transmission with acoustic waves still suffers from the inherent deficiency of limited frequency bandwidth due to the low speed of sound. Over the past few decades, substantial efforts have been made to enhance the capacity of acoustic communication with various schemes, such as wavelength-division multiplexing (WDM), time-division multiplexing (TDM), and multilevel amplitude- or phase-modulation formats to encode information [7–9]. Unfortunately, even with advanced encoding methods, the acoustic-communication capacity cannot satisfy the rapidly increasing requirements in practice.

Recently, orbital angular momentum (OAM) carried by acoustic vortex beams with helical wavefronts has emerged as an alternative degree of freedom for information encoding, which provides great potential to boost the transmission capacity of acoustic communication [10,11]. This acoustic OAM is described by a phase term, $e^{im\theta}$, where m is the topological charge and θ is the azimuthal angle [12–16], providing intrinsically unbounded orthogonal states. Transfer of the OAM to matter produces torque, which is widely used for particle manipulation and vortex-based tweezers [17–21]. OAM-based acoustic

*xiang@berkeley.edu

multiplexing is demonstrated in both free space [10] and cylindrical waveguides [11], showing the enhancement of the transmission rate by N-fold, where N is the number of vortices. As an essential part of multiplexing communication, the method for information retrieval from the superimposed signal, i.e., the demultiplexing process, determines the ultimate transmission speed of the communication system [22]. In OAM-based multiplexing, demultiplexing requires a precise transformation of the initial overlaid OAM modes into states that do not overlap in space. In optics and microwaves, various techniques are used for OAM mode sorting, such as the application of spatial light modulators, Dammann gratings, q plates, or plasmonic metasurfaces based on spin Hall effect [23–28]. However, the mechanisms of action for q plates and plasmonic metasurfaces are unavailable in acoustics, and the precise control of sound would result in a bulky device if we were to directly translate the spatial modulator or Dammann grating into acoustics [10,11,23,25–28].

Existing approaches for the spatial separation of acoustic vortices and information retrieval rely on active arrays or passive resonant methods [10,11], which impose critical limitations to achieve fast and efficient information decoding. With active detection [10], numerous sensors for field detection and complex algorithms for postprocessing are required, and the received mass of data raise another problem in storage, transfer, and analysis procedures, and thus, hinder information decoding in a simple architecture. When the passive method is used [11], a sequence of resonant elements, successively cascaded in 3D space with a bulky volume, is needed to decouple the different OAM modes, the number of which determines the available number of OAM channels. In addition, the resonant nature of the passive device intrinsically restricts the application to a narrow frequency range. Recently, acoustic metamaterials have become an active field driven by both scientific discoveries and application potentials [29–32], which enable diverse wave manipulation functionalities not found in nature, ranging from cloaking, absorption, superresolution, and anomalous reflection and transmission to actively controllable structures and topological acoustic composites [33–40].

We propose and experimentally implement a passive and nonresonant metasurface to overcome the aforementioned problems in OAM mode sorting for acoustic OAM-based multiplexing. Fast, efficient and parallel OAM state separation is realized with an acoustic parabolic-phased metasurface, which transforms the

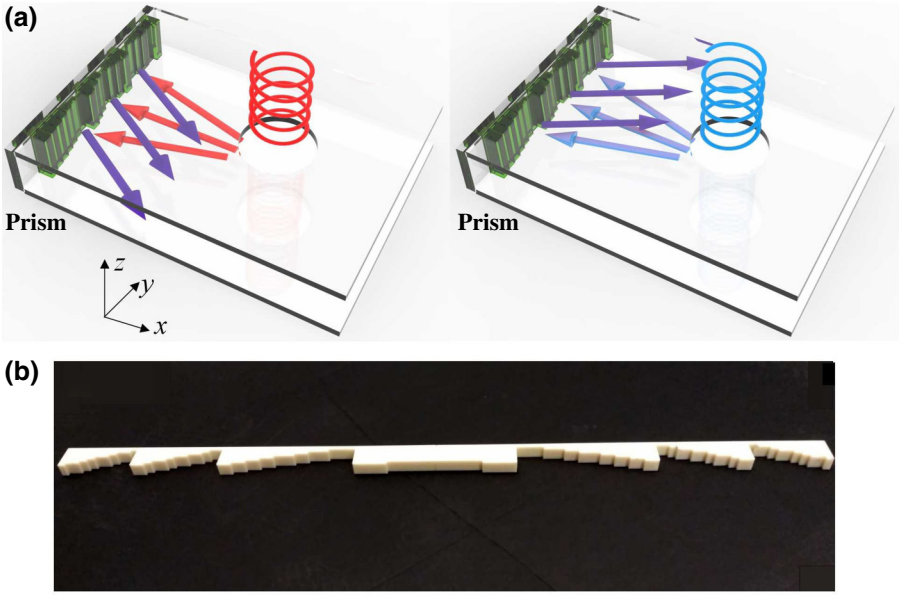

FIG. 1. Parallel sorting of the multiplexed vortex beams with the nonresonant metasurface. (a) Schematic of the experimental setup. Two-dimensional (2D) waveguide (transparent plastic glass) with the subwavelength metasurface (green) assembled on one end serves as a reading device. The metasurface is designed to mimic the phase gradient of a parabolic reflector. Sorting includes two processes. (1) The multiplexed vortex beams propagating in free space (spirals) are coupled into the 2D waveguide through an aperture on the top wall at the focal point of the parabola. (2) The decoding metasurface converts the vortex modes (red and blue arrows) radiated from the focal point into modes with different in-plane linear momenta, resulting in reflected plane waves propagating in different directions (purple arrows). Based on this scheme, information encoded on the superimposed OAM multiplexed signal can be read out in parallel by detecting the reflected waves at specific spatial angles. (b) Photograph of the 3D-printed decoding metasurface used in experiments. The metasurface is made from acrylonitrile butadiene styrene (ABS) plastic, with a length of 89.6 cm in the y direction and maximum thickness of 2.8 cm in the x direction.

helical-phased vortex beams into plane waves with different transverse phase gradients, i.e., different in-plane linear momenta. The lateral phase gradient further diffracts waves with various reflected angles [32–38], depending on the sign and magnitude of the topological charge, m. A theoretical interpretation is developed to analytically prove the intrinsic linear feature between the reflected angle and OAM charge. Remarkably, the advantage of the nonresonant nature of the parabolic geometry mechanism provides the potential to work over a broad bandwidth by employing an appropriate metasurface, and control of the reflected angle is achieved by adjusting the parameters to enable the flexibility to control the sorting resolution on demand. Although we conceptually demonstrate the results for airborne sound, due to laboratory limitations, our scheme provides a paradigm for underwater communication, which is, in principle, implementable in an underwater environment by employing appropriate materials. The proposed OAM sorting method will contribute to increasing the speed of acoustic communication with a simple device, and thus, provides great potential for profound impact on relevant fields.

II. DESIGN OF THE ACOUSTIC OAM DECODING METASURFACE

Parallel sorting of acoustic OAM modes is realized by a geometric configuration based on a parabolic reflector. To avoid the bulky volume of the parabola, while mimicking its function with a planar, thin, and compact device, a subwavelength metasurface is designed to have a thickness profile with different depths of grooves along the surface, which provide the specific phase gradient of the parabola [as shown in Fig. 1(b)]. The width of each groove in the metasurface is $\lambda/8$ in the y direction, and the groove with depth h provides a phase delay of $\phi = 2kh$ (λ is the wavelength and k is the wave number of incident sound). The metasurface is assembled on one end of a two-dimensional waveguide, and the waveguide with the decoding metasurface serves as a reading device in demultiplexing. The concept of our approach is schematically shown in Fig. 1(a), where OAM-mode sorting consists of two processes. In the first step, the multiplexed vortex beams propagating in the free space [indicated by the spirals in Fig. 1(a)] are coupled into the 2D waveguide through an aperture on the top waveguide wall and located in the focal point of the virtual parabola. In the second step, for acoustic vortex beams radiating from the focal point [red and blue arrows in Fig. 1(a)], the decoding metasurface acts as a convertor to transfer the various OAM states into modes with different transverse linear momentum $dk_y \propto (m/p)$ (p is a geometric parameter of the parabola), which results in the reflected plane waves propagating in different angular directions [purple arrows in Fig. 1(a)], according to the sign and magnitude of OAM charge, m. Based on this scheme, the initial superimposed OAM modes are decoupled and the

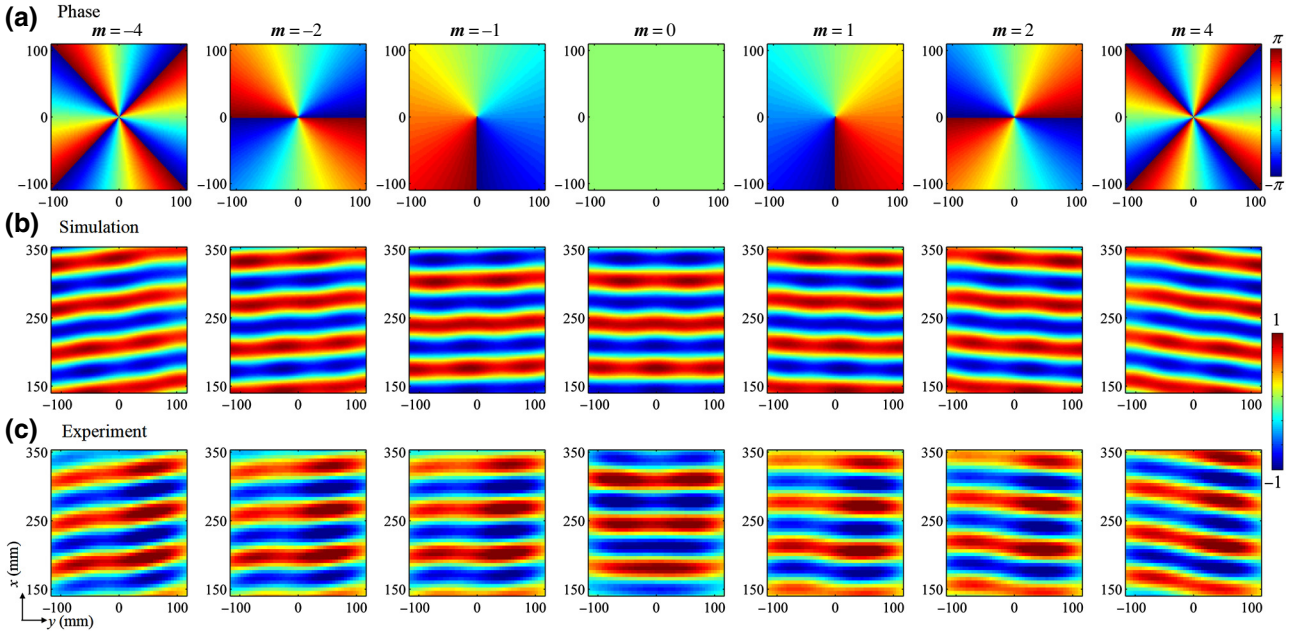

FIG. 2. Parallel sorting of acoustic OAM modes. (a) Simulated phase distributions of acoustic vortex beams with various OAM charges, $m = 0, \pm1, \pm2, \pm4$. The twist number in the phase pattern indicates the magnitude of m, and the twist direction determines the sign. (b),(c) Reflected pressure fields for acoustic vortex beams carrying different OAM charges in numerical simulations and experimental measurements. The simulations and measurements match each other, both of which show that vortex beams with positive and negative OAM charges are reflected in opposite directions, and the reflection angle increases with the magnitude of m. Spatial separation of different acoustic OAM modes is used for parallel information decoding in acoustic OAM-based multiplexing.

information encoded on the multiplexed channels can be simultaneously read out by detecting the waves in specific spatial angles reflected by the single metasurface.

III. EXPERIMENTAL MEASUREMENTS

The experiment is performed in a 2D acoustic waveguide (1×1.2 m^2) filled with air (mass density 1.21 kg/m^3 and sound speed 343 m/s) to demonstrate the parallel sorting of OAM modes. To mimic the incidence of vortex beams from the free space and their coupling to the waveguide, a transducer array is assembled outside the waveguide and above the focal point, consisting of three rings of speakers (with 4, 8, and 16 speakers equally spaced in each ring with radii of 1.2, 2.8, and 4 cm, respectively). Vortex beams with different topological charge, m, are coupled into the waveguide through an aperture (radius of 4 cm) centered in the focal point and then acoustic waves radiate from the aperture. The waveguide walls are formed by acrylic plates and treated as solids for airborne sound, and the acoustic decoding metasurface is 3D-printed from ABS plastic (mimics the parabola with the parameter $p = 0.8$ m). A microphone with a radius of 2.5 mm is used to detect the reflected fields of the decoding metasurface. We conduct the 2D field scanning (234×213 mm^2 with a distance 140 mm from the metasurface and a scanning step 5.1 mm in both x and y directions) to exactly determine the reflected angle, due to the limited propagation distance in the waveguide. However, in practical application, as the finite dimension of the metasurface, the reflected beams of finite width and different angles will nearly not interfere with each after a long propagation distance, and the information encoded in the vortex beams with different m can be directly detected by a single microphone placed at different specific angles.

The phase distributions of acoustic vortex beams carrying different OAM charges, m, are illustrated in Fig. 2(a), where the twist number indicates the magnitude of m and the spiral direction determines the sign. Figure 2(c) shows the experimentally measured reflected pressure fields for

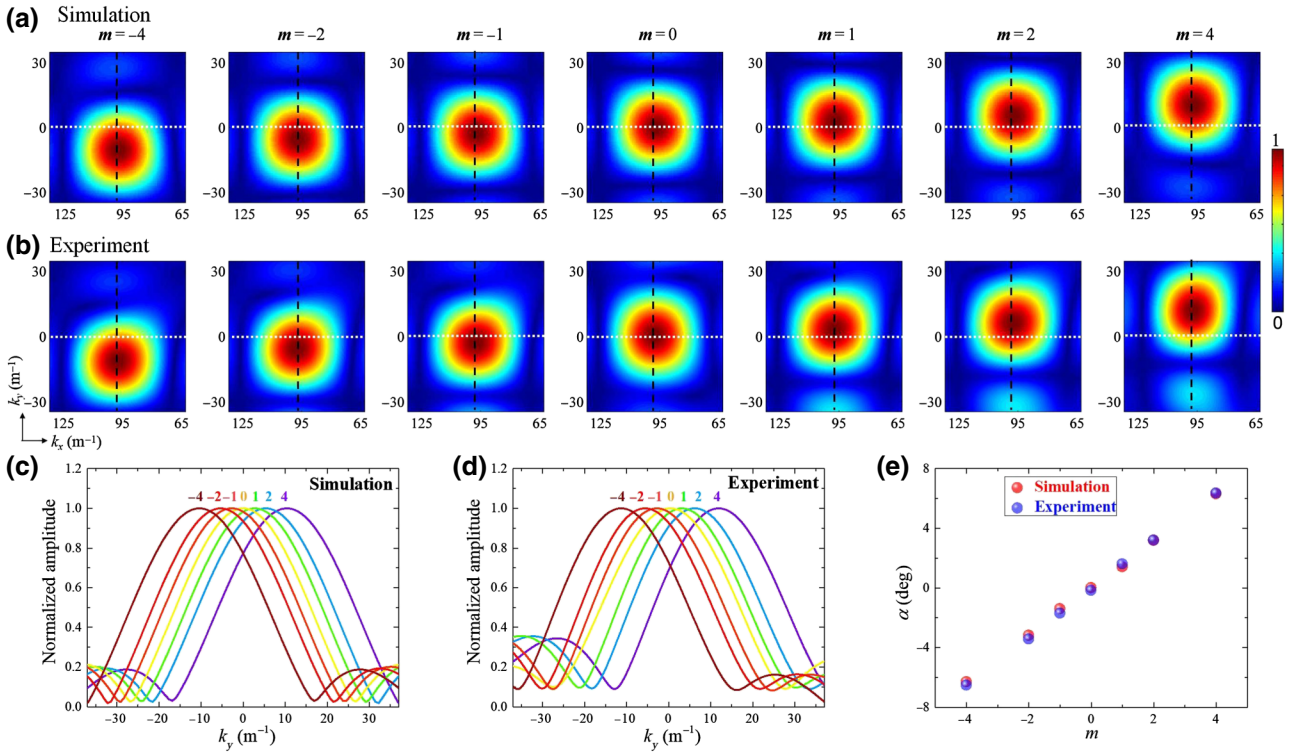

FIG. 3. Analysis of reflection in reciprocal space. (a),(b) Simulated and measured distributions of spectra in reciprocal space with various OAM charges, $m = 0, \pm1, \pm2, \pm4$. The spectrum of the beam with $m = 0$ has only a wavevector component along the propagating direction (x axis), while the nontrivial OAM charge gives rise to the transverse linear momentum, corresponding to the emergence of k_y. The dotted (white) lines show the reference positions $k_y = 0$ and the dashed (black) lines indicate the positions where k_x reaches its maximum value. (c),(d) Distributions of the amplitude of the spectra along the dashed (black) lines in the reciprocal space as functions of k_y for various OAM charges, as obtained from numerical simulations and experimental measurements. The emergence of transverse linear momentum and shift of the spatial spectra for nontrivial m are clearly demonstrated. The results are normalized with their corresponding maximum values. (e) Relationship between the reflection angle, α, and OAM charge, m. The reflection angle results from the transverse linear momentum by $\alpha = \tan^{-1}(k_y/k_x)$. A nearly linear relationship between α and m is observed from both numerical simulations and experimental measurements.

$m = 0, \pm1, \pm2, \pm4$ at 5359 Hz (corresponding to a wavelength of $\lambda = 6.5$ cm), which are confirmed with the simulations shown in Fig. 2(b). The numerical simulations are performed based on the COMSOL Multiphysics pressure acoustics module for reassembling the experimental setup. For a wave emitted by a point source without OAM ($m = 0$), the reflection from the decoding metasurface is a plane wave propagating along the x direction, owing to the parabolic geometry. For vortex beams with nonzero m, different angular momenta of the incident beams are converted into various in-plane linear momenta of the reflected beams by the metasurface, which correspond to different transverse phase gradients of the reflection and further induce angular shifts of the reflected plane waves. As a result, acoustic vortices with different OAM charges are coupled into the plane waves with different reflected angles, as shown in Figs. 2(b) and 2(c), and thus, enable the spatial separation and efficient sorting of OAM modes.

IV. CALCULATION OF REFLECTION IN RECIPROCAL SPACE

To characterize the OAM mode separation, we apply the spatial Fourier transform to map the real space fields into reciprocal space. Figures 3(a) and 3(b) show the spectra of simulated and experimental reflection fields, respectively, with OAM charges of $m = 0, \pm1, \pm2, \pm4$. The spectrum of the $m = 0$ beam has zero wavevector component along the y axis, i.e., $k_y = 0$, which agrees with the above discussion. The emergence of nontrivial m leads to a spectral shift and gives rise to a nonzero linear momentum, k_y, in the transverse direction, inducing a biased angle, α, of the reflection from the x axis. The spectra along the dashed (black) lines (representing the position of maximum k_x in each case) in Figs. 3(a) and 3(b) are plotted in Figs. 3(c) and 3(d). The reflected angle α is calculated from $\alpha = \tan^{-1}(k_y/k_x)$, which is observed to have a nearly linear relationship with OAM charge m, as shown from both simulation and experimental results [Fig. 3(e)]. This intrinsic linear feature between α and m serves as the primary principle for efficient and parallel spatial sorting of different OAM states through the decoding metasurface.

V. THEORETICAL INTERPRETATION AND CONTROLLABILITY BY ADJUSTING PARAMETERS

The principle of fast and parallel OAM sorting based on the parabolic geometry can be analyzed with acoustic ray theory. The virtual parabola mimicked by the subwavelength metasurface is given by $y^2 = 2px$, where p is a geometric parameter that determines the parabolic shape. Given that the distance from a point, $A(x_0, y_0)$, on the parabola to the focal point, $F(p/2, 0)$, is equal to the distance between A and the directrix, $x = -p/2$, i.e., $|AA'| = |AF|$, as shown in Fig. 4(a), the reflection of an omnidirectional point source located at F is identical to the wave radiated from a uniform line source on the directrix, which is a plane wave propagating parallel to the x direction. For vortex beams carrying nontrivial OAM charge m, since the radius of the aperture is much smaller than the distance from the focal point F, the phase of the sound wave impinging on point A can be approximated as $\phi(A) = k|AF| + \phi(\theta)$, where $\phi(\theta)$ is a phase term induced by the OAM. The additional phase $\phi(\theta) = m\theta$ corresponds to the spiral phase term of the vortex beam, with an azimuthal angle of $\theta = \sin^{-1}[y/(y^2/2p + p/2)]$.

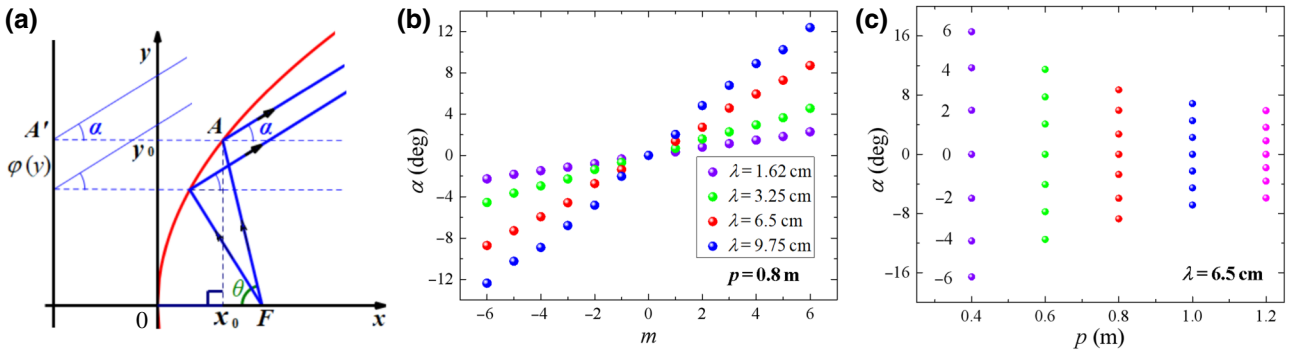

FIG. 4. Analytical model and controllability of the reflection angle. (a) Schematic plot of the ray trajectory of vortex beams radiated from the focal point $F(p/2, 0)$ and reflected by the parabola. The reflection of the vortex beams with nontrivial OAM charge by the parabola is equivalent to a line source with the phase gradient $\varphi(y)$ on the directrix, $x = -p/2$, inducing a transverse linear momentum (along the y axis) and angular shift of the reflection. (b) Reflection angle α as a function of OAM charge m, with wavelengths of the vortex beams of $\lambda = 1.62$, 3.25, 6.5, and 9.75cm and the geometric parameter of the parabola $p = 0.8$m, which is obtained from numerical simulations. The reflection angle shows a linear relationship with both m and λ, i.e., $\alpha \propto m\lambda$, which agrees with the analytical calculation. (c) Relationship between reflection angle $\alpha$and parameter p, with OAM charges $m = 0, \pm2, \pm4, \pm6$ and a wavelength $\lambda = 6.5$ cm, which shows that the angular shift is inversely proportional to p, i.e., $\alpha \propto p^{-1}$. The red dots in (b),(c) represent the results obtained with the same parameters used in the experiments.

In this case, the reflection is equivalent to a wave radiated from the line source with a transverse phase distribution, $\phi(y) = m\theta$, on the directrix. Furthermore, according to the generalized Snell law, the reflection angle, α, is determined by $k\sin(\alpha) = d\phi(y)/dy$, which can be simplified to $\alpha \propto (1/\pi)(\lambda m/p)$ using the first-order Taylor expansion, under the paraxial approximation. The transverse linear momentum induced by the angular momentum is then calculated as $dk_y \propto (m/p)$. These equations explicitly show that the reflection angle, α, increases linearly with the OAM charge, m, and wavelength, λ, whereas it is inversely proportional to the geometric parameter, p. For a sound wave with a given OAM charge m and wavelength λ, the reflection angle, α, can be increased by decreasing the geometrical parameter, p. These analytical results are verified by numerical simulations with the parabolic boundary, as shown in Figs. 4(b) and 4(c), where the relationships between α, m, λ, and p are demonstrated (the red dots represent the results obtained with the same parameters used in experiments). The performances based on the parabolic scheme from 3517 to 21 108 Hz (corresponding to $\lambda = 9.75$ cm to $\lambda = 1.62$ cm) maintain a similar linear relationship with different proportionality constants, as a result of the nonresonant nature of the parabolic geometric mechanism, which indicates the potential for fast and parallel information readout over a broad frequency band. Meanwhile, the analytical derivation also shows the possibility of tuning the slope of the linear relationship for an arbitrarily given m or λ by changing the parameter p. Thus, the angular resolution of the spatial separation for different OAM charges can be optimized by judicious design of the geometry.

VI. CONCLUSION

The parallel sorting of acoustic vortex beams with various OAM charges, m, through a parabolic-phased metasurface provides the ability for fast information decoding in acoustic OAM-based multiplexing. An intrinsic linear feature between the angular separation and OAM charge is obtained in experiments and rigorously proven by analytical derivation under the paraxial approximation. Remarkably, the spatial separation can be flexibly controlled by designing the geometric parameter. Furthermore, although OAM sorting by the metasurface utilized here works over a relatively narrow band due to spatial discretization, the implementation of the parabolic mechanism is not restricted by this specific metasurface, and the nonresonant nature of the parabolic mechanism, in principle, yields a potential for applications over a broad frequency range. The employment of other types of acoustic metasurface could enable a broader bandwidth with more compact devices [41–43]. With the advantage of fast and parallel read-out capability, single-structured simplicity, ray-physics-based design, and controllability, the parallel sorting of acoustic OAM modes with the decoding metasurface will further improve throughput in high-speed acoustic multiplexing, which is important for underwater exploration and communication.

ACKNOWLEDGMENT

This work is supported by the Gordon and Betty Moore Foundation and the King Abdullah University of Science and Technology Office of Sponsored Research (OSR) (award OSR-2016-CRG5-2950-03). X.J. acknowledges support from the Youth Program of the National Natural Science Foundation of China (Grant No. 11904055).

[1] M. Stojanovic. Recent advances in high-speed underwater acoustic communication, IEEE J. Oceanic Eng. **21**, 12 (1996).
[2] T. I. Quickenden and J. A. Irvin. The ultraviolet absorption spectrum of liquid water, J. Chem. Phys. **72**, 4416 (1980).
[3] G. M. Hale and M. R. Querry. Optical constants of water in the 200-nm to 200-μm wavelength region, Appl. Opt., AO **12**, 555 (1973).
[4] C. J. Funk. Multiple scattering calculations of light propagation in ocean water, Appl. Opt., AO **12**, 301 (1973).
[5] M. A. Ainslie and J. G. McColm. A simplified formula for viscous and chemical absorption in sea water, J. Acoust. Soc. Am. **103**, 1671 (1998).
[6] W. S. Pegau, D. Gray, and J. R. V. Zaneveld. Absorption and attenuation of visible and near-infrared light in water: dependence on temperature and salinity, Appl. Opt., AO **36**, 6035 (1997).
[7] H. C. Song and W. S. Hodgkiss. Efficient use of bandwidth for underwater acoustic communication, J. Acoust. Soc. Am. **134**, 905 (2013).
[8] M. Stojanovic, J. A. Catipovic, and J. G. Proakis. Phase-coherent digital communications for underwater acoustic channels, IEEE J. Oceanic Eng. **19**, 100 (1994).
[9] L. Freitag, M. Stojanovic, S. Singh, and M. Johnson. Analysis of channel effects on direct-sequence and frequency-hopped spread-spectrum acoustic communication, IEEE J. Oceanic Eng. **26**, 586 (2001).
[10] C. Shi, M. Dubois, Y. Wang, and X. Zhang. High-speed acoustic communication by multiplexing orbital angular momentum, PNAS **114**, 7250 (2017).
[11] X. Jiang, B. Liang, J.-C. Cheng, and C.-W. Qiu. Twisted acoustics: metasurface-enabled multiplexing and demultiplexing, Adv. Mater. **30**, 1800257 (2018).
[12] B. T. Hefner and P. L. Marston. An acoustical helicoidal wave transducer with applications for the alignment of ultrasonic and underwater systems, J. Acoust. Soc. Am. **106**, 3313 (1999).
[13] X. Jiang, Y. Li, B. Liang, J. Cheng, and L. Zhang. Convert Acoustic Resonances to Orbital Angular Momentum, Phys. Rev. Lett. **117**, 034301 (2016).
[14] X. Jiang, J. Zhao, S. Liu, B. Liang, X. Zou, J. Yang, C.-W. Qiu, and J. Cheng. Broadband and stable acoustic vortex emitter with multi-arm coiling slits, Appl. Phys. Lett. **108**, 203501 (2016).

[15] S. Wang, G. Ma, and C. T. Chan. Topological transport of sound mediated by spin-redirection geometric phase, Sci. Adv. **4**, eaaq1475 (2018).
[16] L. Ye, C. Qiu, J. Lu, K. Tang, H. Jia, M. Ke, S. Peng, and Z. Liu. Making sound vortices by metasurfaces, AIP Adv. **6**, 085007 (2016).
[17] A. Marzo, S. A. Seah, B. W. Drinkwater, D. R. Sahoo, B. Long, and S. Subramanian. Holographic acoustic elements for manipulation of levitated objects, Nat. Commun. **6**, 1 (2015).
[18] D. Baresch, J.-L. Thomas, and R. Marchiano. Observation of a Single-Beam Gradient Force Acoustical Trap for Elastic Particles: Acoustical Tweezers, Phys. Rev. Lett. **116**, 024301 (2016).
[19] A. Marzo, M. Caleap, and B. W. Drinkwater. Acoustic Virtual Vortices with Tunable Orbital Angular Momentum for Trapping of Mie Particles, Phys. Rev. Lett. **120**, 044301 (2018).
[20] L. Zhang. Reversals of Orbital Angular Momentum Transfer and Radiation Torque, Phys. Rev. Appl. **10**, 034039 (2018).
[21] M. Baudoin, J.-C. Gerbedoen, A. Riaud, O. B. Matar, N. Smagin, and J.-L. Thomas. Folding a focalized acoustical vortex on a flat holographic transducer: miniaturized selective acoustical tweezers, Sci. Adv. **5**, eaav1967 (2019).
[22] G. C. G. Berkhout, M. P. J. Lavery, J. Courtial, M. W. Beijersbergen, and M. J. Padgett. Efficient Sorting of Orbital Angular Momentum States of Light, Phys. Rev. Lett. **105**, 153601 (2010).
[23] J. Wang, J.-Y. Yang, I. M. Fazal, N. Ahmed, Y. Yan, H. Huang, Y. Ren, Y. Yue, S. Dolinar, M. Tur, and A. E. Willner. Terabit free-space data transmission employing orbital angular momentum multiplexing, Nat. Photonics **6**, 488 (2012).
[24] T. Lei, M. Zhang, Y. Li, P. Jia, G. N. Liu, X. Xu, Z. Li, C. Min, J. Lin, C. Yu, H. Niu, and X. Yuan. Massive individual orbital angular momentum channels for multiplexing enabled by dammann gratings, Light Sci. Appl. **4**, e257 (2015).
[25] E. Nagali, F. Sciarrino, F. De Martini, L. Marrucci, B. Piccirillo, E. Karimi, and E. Santamato. Quantum Information Transfer from Spin to Orbital Angular Momentum of Photons, Phys. Rev. Lett. **103**, 013601 (2009).
[26] N. Zhang, X. C. Yuan, and R. E. Burge. Extending the detection range of optical vortices by dammann vortex gratings, Opt. Lett., OL **35**, 3495 (2010).
[27] H. Ren, X. Li, Q. Zhang, and M. Gu. On-chip noninterference angular momentum multiplexing of broadband light, Science **352**, 805 (2016).
[28] G. Li, M. Kang, S. Chen, S. Zhang, E. Y.-B. Pun, K. W. Cheah, and J. Li. Spin-enabled plasmonic metasurfaces for manipulating orbital angular momentum of light, Nano Lett. **13**, 4148 (2013).
[29] N. Yu, P. Genevet, M. A. Kats, F. Aieta, J.-P. Tetienne, F. Capasso, and Z. Gaburro. Light propagation with phase discontinuities: generalized laws of reflection and refraction, Science **334**, 333 (2011).
[30] G. Ma and P. Sheng. Acoustic metamaterials: from local resonances to broad horizons, Sci. Adv. **2**, e1501595 (2016).
[31] B. Assouar, B. Liang, Y. Wu, Y. Li, J.-C. Cheng, and Y. Jing. Acoustic metasurfaces, Nat. Rev. Mater. **3**, 460 (2018).
[32] Y. Xie, W. Wang, H. Chen, A. Konneker, B.-I. Popa, and S. A. Cummer. Wavefront modulation and subwavelength diffractive acoustics with an acoustic metasurface, Nat. Commun. **5**, 5553 (2014).
[33] Y. Li, X. Jiang, B. Liang, J. Cheng, and L. Zhang. Metascreen-Based Acoustic Passive Phased Array, Phys. Rev. Appl. **4**, 024003 (2015).
[34] N. Mohammadi Estakhri and A. Alù. Wave-Front Transformation with Gradient Metasurfaces, Phys. Rev. X. **6**, 041008 (2016).
[35] A. Díaz-Rubio, V. S. Asadchy, A. Elsakka, and S. A. Tretyakov. From the generalized reflection law to the realization of perfect anomalous reflectors, Sci. Adv. **3**, 1602714 (2017).
[36] Y. Li, X. Jiang, R. Li, B. Liang, X. Zou, L. Yin, and J. Cheng. Experimental Realization of Full Control of Reflected Waves with Subwavelength Acoustic Metasurfaces, Phys. Rev. Appl. **2**, 064002 (2014).
[37] J. Li, C. Shen, A. Díaz-Rubio, S. A. Tretyakov, and S. A. Cummer. Systematic design and experimental demonstration of bianisotropic metasurfaces for scattering-free manipulation of acoustic wavefronts, Nat. Commun. **9**, 1342 (2018).
[38] J. Li, A. Díaz-Rubio, C. Shen, Z. Jia, S. Tretyakov, and S. Cummer. Highly Efficient Generation of Angular Momentum with Cylindrical Bianisotropic Metasurfaces, Phys. Rev. Appl. **11**, 024016 (2019).
[39] X. Jiang, B. Liang, R. Li, X. Zou, L. Yin, and J. Cheng. Ultra-broadband absorption by acoustic metamaterials, Appl. Phys. Lett. **105**, 243505 (2014).
[40] B. Xie, K. Tang, H. Cheng, Z. Liu, S. Chen, and J. Tian. Coding acoustic metasurfaces, Adv. Mater. **29**, 1603507 (2017).
[41] Y. Li, B. Liang, Z. Gu, X. Zou, and J. Cheng. Reflected wavefront manipulation based on ultrathin planar acoustic metasurfaces, Sci. Rep. **3**, 2546 (2013).
[42] G. Memoli, M. Caleap, M. Asakawa, D. R. Sahoo, B. W. Drinkwater, and S. Subramanian. Metamaterial bricks and quantization of meta-surfaces, Nat. Commun. **8**, 14608 (2017).
[43] B. Liang, J. Cheng, and C.-W. Qiu. Wavefront manipulation by acoustic metasurfaces: from physics and applications, Nanophotonics **7**, 1191 (2018).